Influence of the structure of trigonal mo-v-m3rd oxides (m3rd=-, fe, cu, w) on catalytic performances in selective oxidations of ethane, acrolein, and allyl alcohol

Satoshi Ishikawa, Toru Murayama, Benjamin Katryniok, Franck Dumeignil, Marcia-Carolina Araque Marin, Svetlana Heyte Dyshlovenko, Sébastien Paul, Yudai Yamada, Mizuki Iwazaki, Nagisa Noda, et al.

Influence of the structure of trigonal Mo-V-M3rd oxides (M3rd = -, Fe, Cu, W) on catalytic performances in selective oxidations of ethane, acrolein, and allyl alcohol

Satoshi Ishikawa[a,b], Toru Murayama[b,c], Benjamin Katryniok[d], Franck Dumeignil[d], Marcia Araque[d], Svetlana Heyte[d], Sébastien Paul[d], Yudai Yamada[a], Mizuki Iwazaki[a], Nagisa Noda[a], Wataru Ueda[a, b]

[a] Department of Material and Life Chemistry, Faculty of Engineering, Kanagawa University, 3-27, Rokkakubashi, Kanagawa-ku, Yokohama 221-8686, Japan

[b] Institute of Catalysis, Hokkaido University, N20W10 Kita-ku, Sapporo, Hokkaido 001-0020, Japan

[c] Research Center for Gold Chemistry, Tokyo Metropolitan University, 1-1 Minami-osawa, Hachioji, Tokyo, 192-0397 Japan

[d] Univ. Lille, CNRS, Centrale Lille, ENSCL, Univ. Artois, UMR 8181 – UCCS – Unité de Catalyse et Chimie du Solide, F-59000 Lille, France

E-mail: sishikawa@kanagawa-u.ac.jp, uedaw@kanagawa-u.ac.jp; Tel: +81 45 481 5661

Abstract

Crystalline “MoVO”, “MoVCuO”, “MoVFeO” and “MoVWO” catalysts with a trigonal symmetry were successfully synthesized and characterized. The influence of the as-obtained structures on catalytic performances in selective oxidation reactions was investigated. MoVFeO and MoVCuO accomodated Fe and Cu species inside heptagonal channels, while W in MoVWO was incorporated in pentagonal $\{Mo_6O_{21}\}^{6-}$ units. Whereas MoVO and MoVWO showed catalytic activity in the selective oxidation of ethane and acrolein, MoVFeO and MoVCuO performed very poorly in the same

reaction, suggesting that the presence of empty heptagonal channels is related to ethane and acrolein activations. In the selective oxidation of allyl alcohol, substantial amounts of acrolein (formed by oxidative dehydrogenation) and propanal (formed by isomerization) were formed as primary products over MoVO and MoVWO, whereas MoVFeO and MoVCuO preferentially promoted the formation of acrolein. It was found that the local crystal structure around the heptagonal channel was related with a modification of the reaction pathway for the selective oxidation of allyl alcohol. Due to the prevention of isomerization over MoVFeO, a high acrylic acid yield of 83.1% from allyl alcohol was achieved at 350 °C over this sample.

1. Introduction

Trigonal Mo_3VO_x (MoVO) has attracted much attention as an effective catalyst for the selective partial oxidation of light alkanes and acrolein [1-4]. Figure 1 shows the crystal structure of MoVO. It consists of a network arrangement based on pentagonal $\{Mo_6O_{21}\}^{6-}$ units and $\{MO_6\}$ (M = Mo, V) octahedra, resulting in the formation of hexagonal and heptagonal channels in the crystal structure. The heptagonal channels form micropores with a diameter of 0.40 nm and act as active sites for alkanes, alcohols, and aldehydes activation [4-7]. Recently, we have successfully synthesized crystalline "Mo-V-M3rd" oxides (MoVFeO and MoVWO) with the same trigonal structure by using a structure-directing agent [8]. MoVFeO contained Fe inside the heptagonal channels while W was located in the pentagonal $\{Mo_6O_{21}\}^{6-}$ units, partially substituting Mo species. Significant effects on the nano-scale crystal structure in the selective oxidation of ethane were clearly demonstrated when using MoVO, MoVFeO, and MoVWO [8].

Acrylic acid is a very important chemical. It is widely used as a precursor for adhesives, paints, and plastics [9-12]. Acrylic acid can be synthesized by various methods including *(1)* selective oxidation of acrolein over Mo-V-based mixed metal oxides [9-12], *(2)* oxidehydration of glycerol

(dehydration of glycerol to produce acrolein followed by oxidation of acrolein) [13-16], *(3)* dehydration of lactic acid [17-19], or *(4)* allyl alcohol oxidation [20]. Among these reactions, acrolein oxidation, glycerol transformation, and lactic acid dehydration have been the most widely studied ones. On the other hand, there are only a few reports about allyl alcohol oxidation. Allyl alcohol can be obtained in high yields from biomass-derived sources such as glycerol and *1,3*-propanediol by an easy procedure [21]. Selective oxidation of allyl alcohol can therefore be considered as a promising way for the sustainable synthesis of acrylic acid. In addition, as it contains two functional moieties (double bond and alcohol), allyl alcohol can undergo various subsequent transformations depending on the applied catalyst [22-25].

In the present study, we investigated the role of the crystal structure of Mo-V-M3rd oxides (M3rd = -, Fe, Cu, W) in the selective oxidations of ethane (alkane), acrolein (aldehyde) and allyl alcohol (alcohol with an allyl group). A significant influence of the local crystal structure of the catalysts was observed, of which the tuning allowed us to enhance the acrylic acid yield. We believe that the results reported herein clearly put in light a specific nano-scale structure-reactivity relationship, which can be used as a design basis of a new generation of catalysts for selective partial oxidation reactions.

2. Experimental

2.1. Synthesis of native trigonal Mo_3VO_x oxide

Trigonal Mo_3VO_x was synthesized by a hydrothermal method. First, 8.828 g of $(NH_4)_6Mo_7O_{24}\cdot 4H_2O$ (Mo: 50 mmol, Wako) were dissolved in 120 mL of distilled water. Separately, an aqueous solution of $VOSO_4$ was prepared by dissolving 3.290 g of hydrated $VOSO_4$ (V: 12.5 mmol, Mitsuwa Chemicals) in 120 mL of distilled water. Both solutions were mixed at ambient temperature and stirred for 10 min. The observed natural pH of the as-prepared solution was 3.2. Then, 3.5 mL of a 2 M H_2SO_4

solution were added to decrease the pH to 2.2, and the acidified solution was stirred for 10 min more. The obtained mixed solution was introduced into an autoclave with a 300 mL Teflon inner vessel containing a thin Teflon sheet with 4000 cm^2, which occupies about half of the Teflon inner vessel space. Then, N_2 was bubbled in the solution to flush out residual oxygen traces. The hydrothermal reaction was carried out at 175 °C for 20 h under static conditions in an electric oven. The formed grey solid was recovered and washed with distilled water before being dried overnight in static air at 80 °C. Then, purification was performed using oxalic acid in order to remove impurities formed together with the crystalline material: To 25 mL of an aqueous solution (0.4 mol L^{-1}, 60 °C) of oxalic acid (Wako), 1 g of the dried material was added and stirred for 30 min and then washed with 500 mL of distilled water after filtration. The sample name after purification was abbreviated as "MoVO". Prior to catalytic testing, MoVO was calcined under static air for 2 h at 400 °C in a muffle oven.

2. 2. Preparation of Mo-V-M3rd oxides (M3rd = Fe, Cu, W)

For synthesizing Mo-V-M3rd oxides (M3rd = Fe, Cu, W), ethylammonium trimolybdate [EATM, $(CH_3CH_2NH_3)_2Mo_3O_{10}$] was used as a Mo source instead of $(NH_4)_6Mo_7O_{24}\cdot 4H_2O$. EATM was prepared as previously reported [8, 26]: First, 21.594 g of MoO_3 (0.150 mol, Kanto) were dissolved in 28.0 mL of a 70% ethylamine solution (ethylamine: 0.300 mol, Wako) further diluted to 35% by adding 28.0 mL of distilled water in order to reduce viscosity. After complete dissolution, the as-obtained solution was evaporated under vacuum conditions ($P/P_0 = 0.03$) at 70 °C. The recovered white solid powder was dried overnight in static air at 80 °C.

Then, the Mo-V-M3rd oxides were prepared. First, 1.799 g of EATM (Mo: 10 mmol) were dissolved in 20 mL of distilled water, and an aqueous solution of $VOSO_4$ was prepared by dissolving 0.658 g of hydrated $VOSO_4$ (V: 2.5 mmol) in 20 mL of distilled water. Both solutions were mixed at ambient temperature and stirred for 10 min before addition of 0.301 g of $Fe(NH_4)(SO_4)_2\cdot 12H_2O$ (Fe:

0.625 mmol, Wako), 0.035 g of $Cu(NH_4)_2Cl_4 \cdot 2H_2O$ (Cu: 0.125 mmol, Wako) or 0.160 g of $(NH_4)_6[H_2W_{12}O_{40}] \cdot nH_2O$ (W: 0.625 mmol, Nippon Inorganic Colour and Chemical Co., Ltd.). The pH value changed from 2.4 to 2.0 upon addition of $Fe(NH_4)(SO_4)_2 \cdot 12H_2O$, but no pH change was observed upon addition of $Cu(NH_4)_2Cl_4 \cdot 2H_2O$ or $(NH_4)_6[H_2W_{12}O_{40}] \cdot nH_2O$ (value stable at 2.4). Afterwards, hydrothermal treatment, drying and purification steps were performed in the same way as those described above for MoVO preparation. The obtained materials were abbreviated as "MoVFeO", "MoVCuO" and "MoVWO", respectively. Prior to catalytic tests, the materials were calcined under static air for 2 h at 400 °C in a muffle oven.

2. 3. Characterizations

The synthesized materials were characterized by the following techniques:

- Powder XRD patterns were recorded with a diffractometer (RINT Ultima+, Rigaku) using Cu-Kα radiation (tube voltage: 40 kV, tube current: 40 mA).

- For XRD measurements, the prepared samples were ground for 5 min with Si standard in order to correct the peaks' positions and to exclude any orientation effect. Diffraction patterns were recorded in the 4°~80° 2θ range with 1°/min scan speed. Geometry optimization calculation was carried out using the DMol3 program of Materials Studio 7.1. Perdew-Burke-Ernzerhof (PBE) generalized gradient functional and DND basis set were employed. Rietveld refinement was performed for MoVCuO after air calcination at 400 °C for 2 h using Materials Studio 7.1 (Accelrys). The XRD pattern after correcting the peak position with Si was subjected to refinement. A structural model of MoVCuO obtained by the geometry optimization was used for Rietveld refinement. Occupancy of metals was set according to the result of ICP. All metal atom positions were refined. After the refinement of metal positions, oxygen atom positions were refined to set a proper metal-oxygen length.

The pattern parameters were refined to obtain the lowest R_{wp} value. Rietveld analysis parameters and atom positions of MoVCuO are shown in Table S1 and Table S2, respectively.

- Elemental compositions of the samples were determined by ICP-AES (ICPE-9000, Shimadzu).

- STEM-EDX analysis was conducted using an HD-2000 equipement (Hitachi). Prior to analysis, the samples were ultrasonically dispersed in ethanol. The supernatant liquid was dropped on a Ni grid before being dried overnight for analysis.

- N_2 adsorption isotherms at liquid N_2 temperature were recorded using an auto-adsorption system (BELSORP MAX, Nippon BELL). External surface areas and micropore volumes were determined using the *t*-plot method in the *t* range from 0.15 to 0.90. Prior to N_2 adsorption, the catalysts were heat-treated under partial vacuum at 300 °C for 2 h.

2. 4. Catalytic tests

Allyl alcohol selective oxidation tests were performed on the REALCAT platform in a Flowrence® high-throughput unit (Avantium) equipped with 16 parallel milli-fixed-bed reactors (internal diameter: 2.6 mm, length: 300 mm). First, 50 mg of ground and calcined catalyst samples (400 °C for 2 h under static air) were charged in each of the fixed-bed flow reactors and sandwiched between SiC powder layers (particle size: 0.21 mm, Prolabo) and then heated up to reaction temperature under air flow (10 mL.min^{-1}). The air was switched to the reaction gas mixture with the molar composition of allyl alcohol / O_2 / H_2O / (N_2 + He) = 1 / 2.2 / 42.1 / 11.8 (total flow rate: 40 mL.min^{-1}) under a pressure of 2 bars and these conditions were kept for 20 min at each reaction temperature. Then, liquid products were collected every 140 min by trapping at 10 ˚C. After the trap system, the gas flow was analyzed with on-line gas chromatograph Agilent 7890A GC equipped with two TCD and one FID detectors. Molecular Sieve (Agilent) column was used for separation of O_2, N_2 and CO; Haysep Q (Agilent) column was used for separation of H_2O and CO_2 detected using TCD. Poraplot Q (Agilent) column

was used for separation of organic compounds detected by FID. The trapped liquid phase reactant and products were analyzed with GC-FID (ZB-WAX). In any experiment, the carbon balance was always more than 96%.

Selective oxidation of ethane and acrolein were carried out following the procedure described in our previous paper [6, 27]. The reaction conditions are summarized hereafter. Reaction condition of ethane oxidation: reaction temperature, 300 °C; catalyst amount, 0.50 g; C_2H_6 / O_2 / N_2 = 10 / 10 / 80 (total flow rate: 50 mL.min^{-1}); reaction pressure, ambient pressure. Reaction condition of acrolein: reaction temperature, 200~250 °C; catalyst amount, 0.13 g; C_3H_4O / O_2 / H_2O / (N_2 + He) = 1.6 / 8.2 / 24.7 / 65.5 mL.min^{-1} (total flow rate: 48.6 mL.min^{-1}); reaction pressure, ambient pressure.

3. Results and discussion

3.1. Characterization of the solids

We recently reported in details the method of synthesis and characterization data of MoVO, MoVFeO, and MoVWO. In our previous study, the refined crystalline structure revealed that MoVFeO contained Fe inside heptagonal channels with 42% occupancy while W in MoVWO substituted Mo in the pentagonal $\{Mo_6O_{21}\}^{6-}$ unit with 7% occupancy [8]. Therefore, in the present study, we especially report detailed characterization of MoVCuO. Figure S1 shows the XRD patterns of MoVO, MoVFeO, MoVCuO and MoVWO after calcination at 400 °C for 2 h under air atmosphere. All the materials showed XRD patterns derived from that of the trigonal Mo_3VO_x structure without any additional peak potentially relating to crystallized impurities. Figure 2 shows a STEM-mapping image of MoVCuO. It clearly suggests that all the elements are uniformly distributed throughout the rod-shaped crystal. Table 1 shows the elemental compositions of MoVO and MoVCuO, which were evaluated by EDX (rod-shaped crystal) and ICP (whole part). The elemental compositions of MoVCuO estimated by ICP

(Mo / V / Cu = 1 / 0.28 / 0.04) and EDX (1 / 0.28 / 0.06) was almost the same and the V/Mo value was close to that of MoVO (0.32). Since the elemental composition of probed rod-shaped crystal was consistent with the composition of the whole part of this material, it can be assumed that MoVCuO is composed of crystals with the same elemental composition.

Figure S2 shows the structural model of MoVCuO obtained by a geometry optimization calculation. It was found that Cu is located under the bridging oxygen near the trimer unit facing the heptagonal channel with a distorted square planar geometry. We recently reported that orthorhombic Mo_3VO_x (Orth-MoVO), a crystal analogous with MoVO, can accommodate Cu at the structural site under the bridging oxygen in pentamer unit facing to the heptagonal channel with a distorted square planar geometry (Orth-MoVCuO) [27]. The position of Cu in MoVCuO we determined upon geometry optimization is thus quite similar to that previously found for Orth-MoVCuO. Lattice parameters of MoVO and MoVCuO are shown in Table 1. Compared with the lattice parameter of MoVO (trigonal, a = 2.125 nm, c = 0.4007 nm), the lattice parameter of MoVCuO was almost the same for a but an expansion was observed for c (a = 2.126 nm, c = 0.4018 nm). This expansion is considered to be the result of the introduction of Cu at the interstitial spaces between the a-a planes. Similar lattice parameter changes were also previously observed in Orth-MoVO upon introduction of Cu [27].

Rietveld refinement was then carried out for MoVCuO in order to obtain more evidences (Figure 3). The refinement was carried out by using the crystal structure obtained by the geometry optimization calculation as a starting structure. The refinement parameters, atom positions and occupancies are shown in Table S1 and Table S2, respectively. The simulated XRD pattern and recorded XRD pattern fitted well and the R_{wp} value, agreement factor between the observed pattern and the simulation pattern, was 11.2%, indicating reliability of the deduced structural model. Based on these results, we concluded that Cu was actually located under the bridging oxygen near the trimer unit facing the heptagonal channel with a distorted square planar geometry with an occupancy of 28%.

From nitrogen physisorption (Table 2), one can see that the specific surface areas of MoVO, MoVFeO, and MoVWO were roughly the same with 18.0, 15.1 and 16.7 $m^2.g^{-1}$, respectively. MoVCuO showed a comparatively much smaller external surface area (7.0 $m^2.g^{-1}$). Micropore volumes of MoVO and MoVWO were comparable (4.0×10^{-3} and 3.6×10^{-3} $cm^3.g^{-1}$, respectively). On the other hand, the micropore volumes of MoVFeO and MoVCuO were 2.7×10^{-3} and 1.4×10^{-3} $cm^3.g^{-1}$, respectively, which were much smaller than those of MoVO and MoVWO. The difference between MoVO, MoVWO and MoVFeO, MoVCuO is the aforementioned presence of metals inside the heptagonal channels. We previously reported that the empty heptagonal channels work as micropores to adsorb small molecules such as N_2, CO_2, CH_4 or C_2H_6 [1, 4, 7, 28-29]. Accordingly, Fe and Cu in MoVFeO and MoVCuO are thought to block the access of N_2 into the heptagonal channels, resulting in a decrease in micropore volume. Similar decrease in the micropore volume by the introduction of Cu was also observed in Orth-MoVO [27].

3.2. Selective oxidation of ethane and acrolein over the Mo-V-M3rd oxides

The selective oxidation of ethane and acrolein was carried out using four distinct catalysts with the same trigonal Mo_3VO_x host structure in order to evaluate the structure dependency on the reactivity in alkane oxidation and aldehyde oxidation (Table 2). Ethane oxidation was carried out at 300 °C using a molar feed composition of $C_2H_6/O_2/N_2$ = 10/10/80 at a total flow rate of 50 $mL.min^{-1}$. Acrolein oxidation was carried out at 230 °C using a molar feed composition of $C_3H_4O/O_2/H_2O/(He+N_2)$ = 1.6/8.2/24.7/65.5 at a total flowrate of 48.6 $mL.min^{-1}$. Acrolein conversion and acrylic acid selectivity as a function of reaction temperature are shown in Figure S3. It is worth mentioning that the crystal structure of the catalysts was maintained after reaction, as previously observed [1, 11].

In the selective oxidation of ethane at 300 °C, the conversion over MoVO was 19.2% and the

selectivities to ethene, acetic acid and CO_x were 84.7%, 4.3% and 11.0%, respectively. MoVWO showed a slightly lower ethane conversion (12.2%) than MoVO. This lower conversion could be related to the substitution of redox-active Mo species with less redox-active W species. Products' selectivity was similar for MoVO and MoVWO. On the other hand, MoVFeO and MoVCuO were almost inactive for this reaction, with ethane conversions of 1.3% and 2.6% for MoVFeO and MoVCuO, respectively. We have previously reported that ethane is converted to ethene inside the heptagonal channel of MoVO [4-7]. Therefore, the significant drop in the ethane conversion observed by the introduction of Fe and Cu can be ascribed to the inaccessibility of ethane to the heptagonal channels.

In the case of acrolein oxidation (Figure S3), the acrolein conversion was in the order of MoVO ≅ MoVWO > MoVFeO ≫ MoVCuO. At 230 °C, acrolein conversion over MoVO was 71.5% with products' selectivities to acrylic acid, acetic acid and CO_x of 92.0%, 0.5% and 7.5%, respectively. MoVWO showed a slightly lower acrolein conversion (50.5%) than MoVO. In this case, the product selectivity was similar to that of MoVO. MoVFeO showed comparably lower catalytic activity for acrolein oxidation with 25.3% conversion at 230 °C. However, the selectivity to acrylic acid was slightly increased at all the studied reaction temperatures (Figure S3). MoVCuO showed negligible acrolein conversion with 3.4% at 230 °C. It has been reported that acrolein is converted to acrylic acid over the mouth of the heptagonal channels on the catalyst surface [4, 6, 11]. Therefore, it is possible that the location of metals inside the heptagonal channel decreased the catalytic activity by influencing an adsorption and activation of substrate (acrolein and molecular oxygen), a stabilization degree of the reaction intermediate, or a desorption of reaction product (acrylic acid), although the decrease should be at least partly due to the comparatively low specific surface area in the case of MoVCuO. The catalytic activities for selective oxidations of ethane and acrolein were found to be strongly influenced by the location site of additional metals in the crystal structure.

3.3. Selective oxidation of allyl alcohol over the Mo-V-M3rd oxides

Selective oxidation of allyl alcohol was carried out using the four Mo-V-M3rd oxide catalysts. Figure 4 shows the allyl alcohol conversion and product selectivities as a function of contact time at 250 °C, 300 °C and 350 °C. In this case also, the basic crystal structure was maintained after the reaction as confirmed by XRD. Figure 4 (A) shows the allyl alcohol conversion and product selectivities at 250 °C. MoVO and MoVWO showed almost the same allyl alcohol conversion at each contact time, with an increase in conversion with an increase in contact time. Almost full conversion was observed when the contact time reached 2.5×10^{-3} g_{cat}.min.mL^{-1}. Propanal and acrolein were formed as primary products (see Scheme 1) in almost identical quantities over MoVO and MoVWO at a short contact time. With an increase in contact time, propanal and acrolein were sequentially oxidized, resulting in the formation of propionic acid and acrylic acid (see Scheme 1), respectively. MoVFeO showed a slightly lower allyl alcohol conversion than MoVO and MoVWO, and full allyl alcohol conversion was observed when the contact time reached 3.3×10^{-3} g_{cat}.min.mL^{-1}. MoVCuO clearly showed a lower allyl alcohol conversion than the other three catalysts when contact time was short, supposedly linked with its smaller specific surface area, but full conversion was achieved when the contact time was increased to 3.3×10^{-3} g_{cat}.min.mL^{-1}. It is interesting to note that MoVFeO and MoVCuO showed different behaviours compared to MoVO and MoVWO in terms of products' selectivity. At a short contact time, MoVFeO and MoVCuO showed clearly higher acrolein selectivity than that to propanal. Table 3 shows the product selectivities of MoVO, MoVFeO, and MoVWO when allyl alcohol conversion was 74.4~79.3%. The selectivities to allylic compounds (acrolein + acrylic acid) and propanal derivatives (propanal and propionic acid) over MoVO were 47.2% and 49.3%, respectively. In the case of MoVWO, the allylic compounds selectivity and the propanal derivatives'

selectivity were 50.8% and 45.1%, respectively, and were almost the same as those of MoVO. On the other hand, MoVFeO showed much higher selectivity to the allylic compounds (68.7%) than for propanal derivatives (23.2%).

Scheme 1 shows the proposed reaction pathways for the allyl alcohol selective oxidation. Acrolein and propanal are the primary products of allyl alcohol oxidation. Acrolein is formed by oxidative dehydrogenation. Propanal is formed by isomerization *via* either intermolecular hydrogen transfer (from the metal-hydride) or intramolecular hydrogen transfer (*1,3*-hydrogen shift) [24-25, 30-31]. For MoVO, MoVFeO, MoVCuO, and MoVWO, the specific difference in these catalysts was the particular crystal structure around the heptagonal channel, that is to say, that the heptagonal channels of MoVO and MoVWO are empty, while the heptagonal channels of MoVFeO and MoVCuO are occupied by Fe or Cu. Therefore, it is reasonable to assume that the observed selectivity difference between MoVO, MoVWO and MoVFeO, MoVCuO for allyl alcohol oxidation is most likely caused by the structural difference around the heptagonal channels. Actually, we have recently reported the catalytic performance of four distinct Mo_3VO_x catalysts behaving different crystal phases for selective oxidation of allyl alcohol [32]. We found that tetragonal Mo_3VO_x (without heptagonal channels in its crystal structure) preferentially promoted the formation of acrolein as a primary product with almost no propanal being formed, although orthorhombic, trigonal and amorphous Mo_3VO_x (containing empty heptagonal channels in their crystal structure) produced both acrolein and propanal. Another study showed that orthorhombic Mo_3VO_x, structural analogous with MoVO, was able to abstract a hydride from alcohol in the alcohol oxidation, whereby the metals around the empty heptagonal channel were suggested to be responsible for this abstraction [33]. During the isomerization process, abstraction of the hydride from allyl alcohol is an essential step, regardless of the reaction pathway as described above [24, 30]. Based on these facts, we concluded that MoVO and MoVWO having an empty heptagonal channel can operate the isomerization of allyl alcohol in addition to the oxidative

dehydrogenation since the metals around the empty heptagonal channels can abstract the hydride from allyl alcohol. In contrast, MoVFeO and MoVCuO having metals inside the heptagonal channel cannot abstract the hydride from allyl alcohol, resulting in the preferential formation of acrolein. The reason why the metal-occupied heptagonal channel cannot abstract the hydride from allyl alcohol is still not clear, but changes in chemical properties such as the structural flexibility, bond strains, or oxidation states of metals may contribute to this difference. Further works such as kinetics analysis, probe-IR study, and substrates adsorbed TPD are surely necessary for the deep understanding on this selectivity differences. The small amount of propanal formed over MoVFeO and MoVCuO should be due to the empty heptagonal channels of these catalysts since the occupancy of Fe and Cu is not so high (Fe, 42%; Cu, 28%).

Figure 4 (B) shows the catalytic performance of the catalysts at 300 °C as a function of contact time, and Table 3 shows the allyl alcohol conversions and product selectivities over MoVO, MoVFeO, and MoVWO at 300 °C when the allyl alcohol conversion was 60.3~66.3%. The selectivities of the allylic compounds and the propanal derivatives were 57.6% and 39.0% over MoVO and 62.3% and 33.2% over MoVWO, respectively. Also, at 250 °C, MoVO and MoVWO promoted the formation of both allylic compounds and propanal derivatives. The slight decrease in the propanal derivative selectivity compared with that at 250 °C might be due to differences in activation energies of oxidative dehydrogenation (to form acrolein) and isomerization (to form propanal). Actually, it has been reported that propanal was mainly formed as the primary product at a low reaction temperature (below 200 °C) over Mo_3VO_x, while the formation rate of acrolein was increased at a high reaction temperature [32]. When the contact time was increased, intermediately formed acrolein and propanal were sequentially oxidized to acrylic acid and propionic acid, respectively. A further increase in contact time caused the decomposition of acrylic acid and propionic acid, resulting in the formation of acetic acid and CO_x. The maximum yields of acrylic acid over MoVO and MoVWO were 55.7% and 55.3%, respectively.

In the case of MoVFeO and MoVCuO, like for the reaction at 250 °C, the formation of allylic compounds was promoted, and only very small amounts of propanal derivatives were observed. The selectivities to the allylic compounds and propanal derivatives over MoVFeO at this temperature were 77.9% and 17.7%, respectively, when the allylic alcohol conversion was 64.1%. MoVFeO showed an obviously higher acrylic acid yield than MoVO and MoVWO when the contact time was increased, due to the preferential formation of acrolein as the precursor of acrylic acid, and a maximum acrylic acid yield of 73.6% was achieved. In the case of MoVCuO, the catalytic activity for acrolein oxidation was poor compared with that of the other three catalysts, and a longer contact time was needed to oxidize acrolein to acrylic acid. However, such a condition led to further oxidation of the formed acrylic acid, and the maximum acrylic acid yield was thus decreased (54.6%).

At 350 °C, all the catalysts achieved full allyl alcohol conversion at all of the probed contact times. With an increase in contact time, CO_x and acetic acid selectivity was increased due to decomposition of acrylic acid. At this temperature, almost no propanal derivatives were observed for any of the catalysts, probably due to the different activation energy compared to the formation of allylic compounds. At this temperature, the maximum yields to acrylic acid over MoVO, MoVFeO, MoVCuO and MoVWO were 73.3%, 83.1%, 72.6% and 65.2%, respectively. MoVFeO showed a clearly higher acrylic acid yield for the same reason described above. MoVWO showed a slightly lower acrylic acid yield than the other three catalysts. In the case of MoVWO, a significant decrease in acrylic acid selectivity was observed with an increase in contact time. Probably, the presence of W in MoVWO induced and increase in the number of Brønsted acid sites, and such acid sites might have catalyzed the rapid decomposition of acrylic acid, resulting in a decrease in the acrylic acid yield. The acrylic acid yield obtained over MoVFeO was quite high even compared to literature (Pd-Cu/Al_2O_3, 18.4%; Mo-V-W-Cu-Zr oxide, 59.5%; orthorhombic Mo_3VO_x, 73%) [19]. In this experiment, we not only discovered different selectivity behaviour for allyl alcohol oxidation on the basis of the crystal

structure but also obtained quite a high acrylic acid yield by one-pot oxidation of allyl alcohol by modifying the local crystal structure.

4. Conclusions

Four distinct trigonal Mo-V-M3rd oxides (M3rd = -, Fe, Cu, W) were synthesized and characterized. Fe and Cu in MoVFeO and MoVCuO were found to be located in heptagonal channels, while W in MoVWO was located in pentagonal $\{Mo_6O_{21}\}^{6-}$ units, partially substituting Mo atoms. For the selective oxidation of ethane and acrolein, MoVO and MoVWO showed high reactivity, while the catalytic activities of MoVFeO and MoVCuO were low. A significant role of the empty heptagonal channel for these reactions was clearly shown. For the selective oxidation of allyl alcohol, a clear difference in the product selectivity was observed. As primary products of the allyl alcohol oxidation, acrolein and propanal were formed over MoVO and MoVWO by oxidative dehydrogenation and isomerization, respectively. On the other hand, MoVFeO and MoVCuO preferentially promoted the formation of acrolein, and the formation rate of propanal was low. Strong dependence of the crystal structure on product selectivity was hence observed. Due to the prevention of isomerization of allyl alcohol, a maximum acrylic acid yield of 83.1% was achieved over MoVFeO in the selective oxidation of allyl alcohol. This work showed the importance of local crystal structure for substrates with different functional groups, and this important result may be the basis of the design of a new generation of catalysts for selective oxidation reactions.

Acknowledgements

This research was conducted within the frame of the CNRS International Associated Laboratory CAT&P4BIO and then NANOXCAT. The REALCAT platform is benefiting from a state subsidy administrated by the French National Research Agency (ANR) within the frame of the 'Future

Investments' program (PIA), with the contractual reference 'ANR-11-EQPX-0037'. Chevreul Institute (FR 2638), Ministère de l'Enseignement Supérieur, de la Recherche et de l'Innovation, Région Hauts-de-France, CNRS, FEDER, Centrale Lille and Centrale Initiatives Foundation are warmly acknowledged for their financial supports.

References

[1] T. Konya, T. Katou, T. Murayama, S. Ishikawa, M. Sadakane, D. J. Buttrey and W. Ueda, *Catal. Sci. Technol*., 2013, **3**, 380.

[2] M. Sadakane, N. Watanabe, T. Katou, Y. Nodasaka and W. Ueda, *Angew. Chem., Int. Ed.,* 2007, **46**, 1493.

[3] W. D. Pyrz, D. A. Blom, M. Sadakane, K. Kodato, W. Ueda, T. Vogt and D. J. Buttrey, *Chem. Mater*., 2010, **22**, 2033.

[4] S. Ishikawa and W. Ueda, *Catal. Sci. Technol.*, 2016, **6**, 617.

[5] S. Ishikawa, X. Yi, T. Murayama and W. Ueda, *Appl. Catal., A*, 2014, **474**, 10.

[6] S. Ishikawa, X. Yi, T. Murayama and W. Ueda, *Catal. Today*, 2014, **238**, 35.

[7] S. Ishikawa, D. Kobayashi, T. Konya, S. Ohmura, T. Murayama, N. Yasuda, M. Sadakane and W. Ueda, *J. Phys. Chem. C*, 2015, **119**, 7195.

[8] S. Ishikawa, T. Murayama, M. Kumaki, M. Tashiro, Z. Zhang, A. Yoshida, W. Ueda, *Top. Catal.,* 2016, **59**, 1477.

[9] J. Tichy, *Appl. Catal., A,* 1997, **157**, 363.

[10] C. Qiu, C. Chen, S. Ishikawa, T. Murayama and W. Ueda, *Top. Catal*., 2014, **57**, 1163.

[11] C. Chen, K. Nakatani, T. Murayama and W. Ueda, *ChemCatChem*, 2013, **5**, 2869.

[12] T. V. Andrushkevich, *Catal Rev Sci Eng*, 1993, **35**, 213.

[13] K. Omata, K. Matsumoto, T. Murayama and W. Ueda, *Chem. Lett.*, 2014, **43**, 435.

[14] K. Omata, K. Matsumoto, T. Murayama and W. Ueda, *Catal. Today*, 2016, **259**, 205.

[15] X. Li and Y. Zhang, *ACS Catal.*, 2016, **6**, 2785.

[16] A. Chieregato, M. D. Soriano, E. G. González, G. Puglia, F. Basile, P. Concepción, C. Bandinelli,

[17] J. M. L. Nieto and F. Cavani, *ChemSusChem,* 2015, **8**, 398.

[18] B. Yan, L. Z. Tao, Y. Liang and B. Q. Xu, *ACS Catal.*, 2014, **4**, 1931.

[19] V. C. Ghantani, M. K. Dongare and S. B. Umbarkar, *RSC Adv.*, 2014, **4**, 33319.

[20] S. Yang, M. Kim, S. Yang, D. S. Kim, W. J. Lee and H. Lee, *Catal. Sci. Technol.*, 2016, **6**, 3616.

[21] Y. Kon, M. Araque, B. Katryniok, T. Nakashima, J. Thuriot, S. Paul, F. Dumeignil. ChemistrySelect, 2017, **2**, 9864.

[22] X. Li and Y. Zhang, *ACS Catal.*, 2016, **6**, 143.

[23] S. Matsubara, T. Okazoe, K. Oshima and K. Takai, *Bull. Chem. Soc. Jpn.*, 1985, **58**, 844.

[24] V. Cadierno, S. E. G. Garrido, J. Gimeno, A. V. Álvarez and J. A. Sordo, *J. Am. Chem. Soc.*, 2006, **128**, 1360.

[25] M. Ito, S. Kitahara and T. Ikariya, *J. Am. Chem. Soc.*, 2005, **127**, 6172.

[26] S. Ishikawa, T. Murayama, S. Ohmura, M. Sadakane and W. Ueda, *Chem. Mater*., 2013, **25**, 2211.

[27] S. Ishikawa, Y. Yamada, C. Qiu, Y. Kawahara, N. Hiyoshi, A. Yoshida, W. Ueda, *Chem. Mater.* 2019, **31**, 1408.

[28] M. Sadakane, K. Kodato, T. Kuranishi, Y. Nodasaka, K. Sugawara, N. Sakaguchi, T. Nagai, Y. Matsui and W. Ueda, *Angew. Chem., Int. Ed*., 2008, **47**, 2493.

[29] M. Sadakane, S. Ohmura, K. Kodato, T. Fujisawa, K. Kato, K. Shimizu, T. Murayama and W. Ueda, *Chem. Commun*., 2011, **47**, 10812.

[30] R. Uma and C. Crévisy, R. Grée, *Chem. Rev.*, 2003, **103**, 27.

[31] A. V. Romero, A. B. Gómez and B. M. Matute, *ACS. Catal.*, 2015, **5**, 708.

[32] T. Murayama, B. Katryniok, S. Heyte, M. Araque, S. Ishikawa, F. Dumeignil, S. Paul and W.

Ueda, *ChemCatChem*, 2016, **8**, 2415.

[33] F. Wang and W. Ueda, *Appl. Catal., A,* 2008, **346**, 155.

Fig. captions

Figure 1. Structural model of trigonal Mo_3VO_x oxide. Light blue, Mo; gray, V; red, O.

Figure 2. STEM-mapping image of MoVCuO.

Figure 3. (A) Structural model of MoVCuO obtained by Rietvelt refinement. Mo, light blue; V, grey; O, red; mixture of Mo and V, light green; Cu, dark red. The crystal structure in the *c* direction and the local structure around Cu are shown in (B). (C) Difference (black), calculated (blue line), and observed (red) patterns from Rietveld refinement obtained by using XRD data of MoVCuO after air calcination at 400 °C for 2 h. XRD peaks at 27.8°□28.8°, 46.8°□47.7°, 55.7°□56.4°, 68.9°□69.3°, and 76°□76.7° were attributed to powdered Si added in order to remove potential orientation effects and were excluded in Rietveld refinement.

Figure 4. Allyl alcohol conversion (red circles) and product selectivities as a function of contact time at (A) 250 °C, (B) 300 °C, and (C) 350 °C. Blue triangles, acrolein; inverted light green triangles, propanal; blue squares, acrylic acid; dark green diamonds, propionic acid; red right triangles, acetaldehyde; red cross marks in open red squares, acetic acid; red open circles in red open squares, CO_x.

Scheme 1. Reaction pathways for selective oxidation of allyl alcohol to propionic and acrylic acids.

Figure S1. XRD patterns of MoVO (a), MoVFeO (b), MoVCuO (c) and MoVWO (d) after air calcination at 400 °C for 2 h.

Figure S2. Structural model of MoVCuO obtained after geometry optimization (left figure). Mo, light blue; V, grey; O, red; mixture of Mo and V, dark red; Cu, light green. Local structure around Cu is shown in the right figure.

Figure S3. Acrolein conversion (A) and acrylic acid selectivity (B) over MoVO (black

circles), MoVFeO (red squares), MoVCuO (green diamonds) and MoVWO (blue triangles) as a function of reaction temperature.

Table 1. Elemental compositions and lattice parameters of MoVO and MoVCuO

Catalyst	Mo/V/M^{3rd}			Lattice parameters /nm	
	Theoretical	ICP (Bulk)[a]	EDX (rod-shaped crystal)[b]	*a*	*c*
MoVO	1/0.25/-	1/0.32/-	-	2.125	0.4007
MoVCuO	1/0.25/0.06	1/0.28/0.04	1/0.28/0.06	2.126	0.4018

[a] Determined by ICP.
[b] Determined by EDX.

Table 2. Micropore volume, external surface area, and results of the selective oxidation of ethane and acrolein over Mo-V-M3rd oxides

Catalyst	Micropore volume[a] /10^3 cm^3 g^{-1}	External surface area[a] /m^2 g^{-1}	C_2H_6 conv.[b] /%	Selectivity[b] /%			ACR conv.[c] /%	Selectivity[c] /%		
				C_2H_4	AcOH	CO_x		AA	AcOH	CO_x
MoVO	4.0	18.0	19.2	84.7	4.3	11.0	71.5	92.0	0.5	7.5
MoVFeO	2.7	15.1	1.3	82.0	2.4	15.6	25.3	96.2	0.5	3.3
MoVCuO	1.4	7.0	2.8	87.5	2.6	9.9	4.3	92.6	0.0	7.4
MoVWO	3.6	16.7	12.2	88.6	3.3	8.1	50.5	93.2	0.4	6.4

[a] Measured by N_2 adsorption at liq. N_2 temperature and determined by the *t*-plot method.
[b] Reaction conditions: catalyst amount, 0.50 g; reaction temperature, 300 °C; reaction gas mixture, $C_2H_6/O_2/N_2$ = 5/5/40 mL min^{-1}. AcOH, acetic acid.
[c] Reaction conditions: catalyst amount, 0.13 g; reaction temperature, 230 °C; reaction gas mixture, $ACR/O_2/H_2O/(He+N_2)$ = 0.8/4.0/12.0/31.8 mL min^{-1}. ACR, acrolein; AA, acrylic acid; AcOH, acetic acid.

Table 3. Allyl alcohol conversion and product selectivity

Catalyst	Reaction temperature /°C	Contact time /$\times 10^{-3}$ g_{cat}.min.mL^{-1}	AAOH conv.[a] /%	Product selectivity[b] /%						
				ACR	PRP	AA	PA	AcOH	Ace	CO_x
MoVO	250	1.2	79.3	41.2	35.2	6.0	14.1	0.0	0.3	2.9
MoVO	300	0.3	60.3	38.5	23.2	19.1	15.8	0.0	0.2	3.2
MoVFeO	250	2.5	74.4	62.8	17.6	5.9	5.7	0.9	1.8	3.3
MoVFeO	300	0.3	64.1	72.7	12.7	5.2	5.0	0.0	0.6	3.5
MoVWO	250	1.2	76.0	39.1	26.5	11.7	18.6	0.0	0.9	2.2
MoVWO	300	0.3	66.3	40.6	20.2	21.7	13.0	0.0	0.2	4.3

[a] Allyl alcohol conversion.
[b] ACR, acrolein; PRP, propanal; AA, acrylic acid; PA, propionic acid; AcOH, acetic acid; Ace, acetaldehyde.

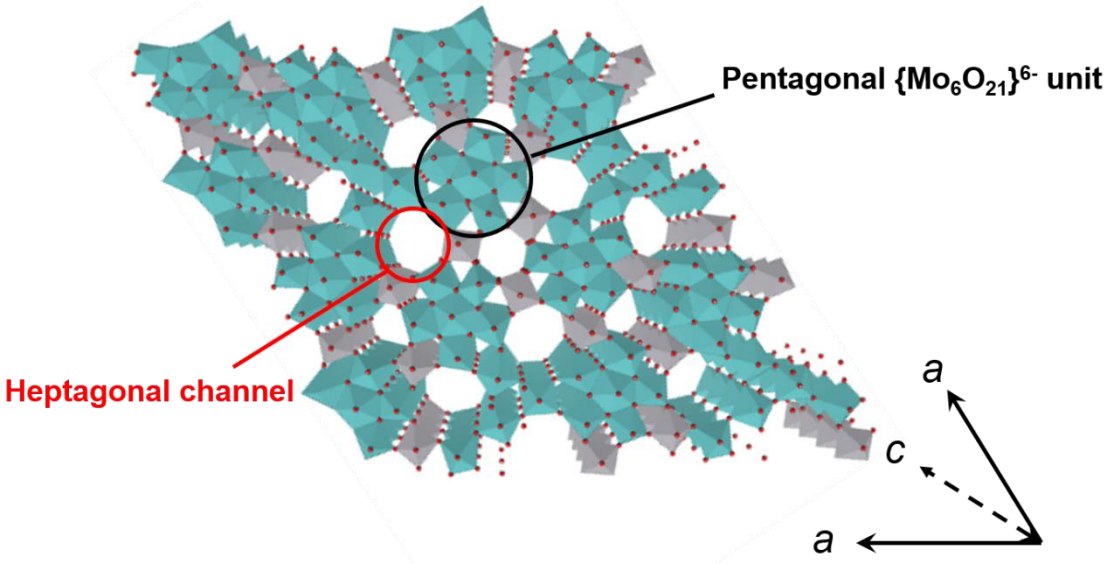

Figure 1. Structural model of trigonal Mo_3VO_x oxide. Light blue, Mo; grey, V; red, O.

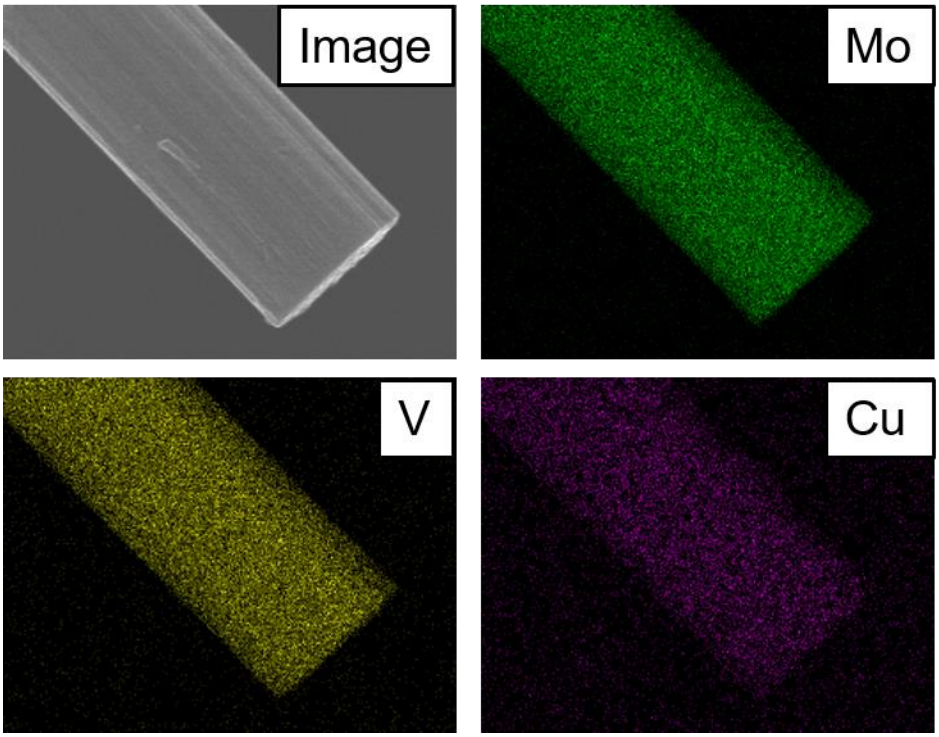

Figure 2. STEM-mapping image of MoVCuO.

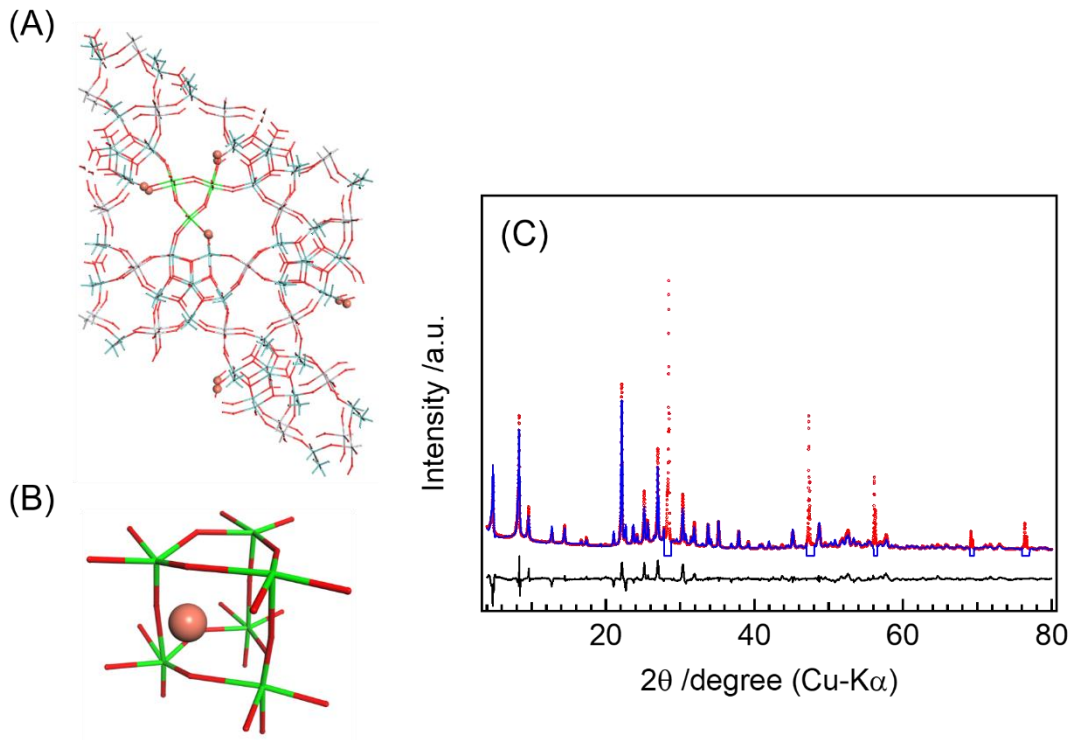

Figure 3. (A) Structural model of MoVCuO obtained by Rietvelt refinement. Mo, light blue; V, grey; O, red; mixture of Mo and V, light green; Cu, dark red. The crystal structure in the *c* direction and the local structure around Cu are shown in (B). (C) Difference (black), calculated (blue line), and observed (red) patterns from Rietveld refinement obtained by using XRD data of MoVCuO after air calcination at 400 °C for 2 h. XRD peaks at 27.8°~28.8°, 46.8°~47.7°, 55.7°~56.4°, 68.9°~69.3°, and 76°~76.7° were attributed to powdered Si added in order to remove potential orientation effects and were excluded in Rietveld refinement.

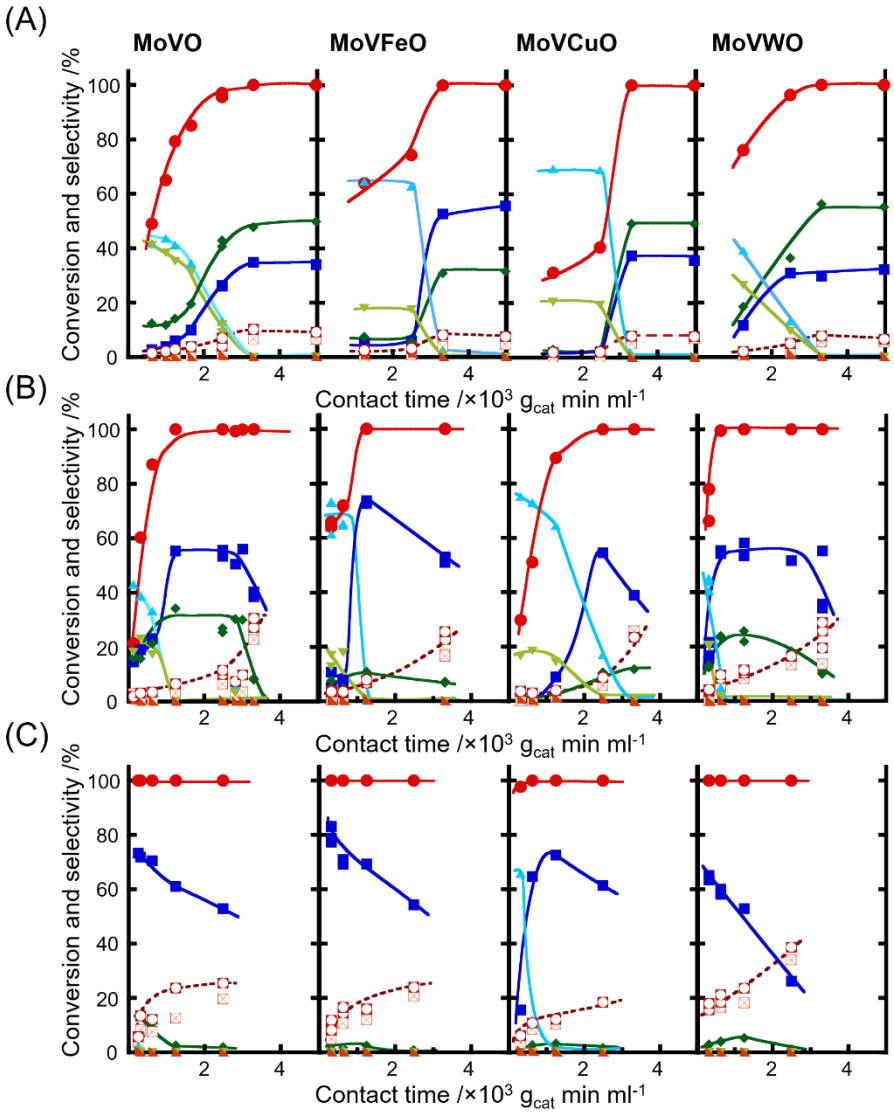

Figure 4. Allyl alcohol conversion (red circles) and product selectivities as a function of contact time at (A) 250 °C, (B) 300 °C, and (C) 350 °C. Blue triangles, acrolein; inverted light green triangles, propanal; blue squares, acrylic acid; dark green diamonds, propionic acid; red right triangles, acetaldehyde; red cross marks in open red squares, acetic acid; red open circles in red open squares, CO_x.

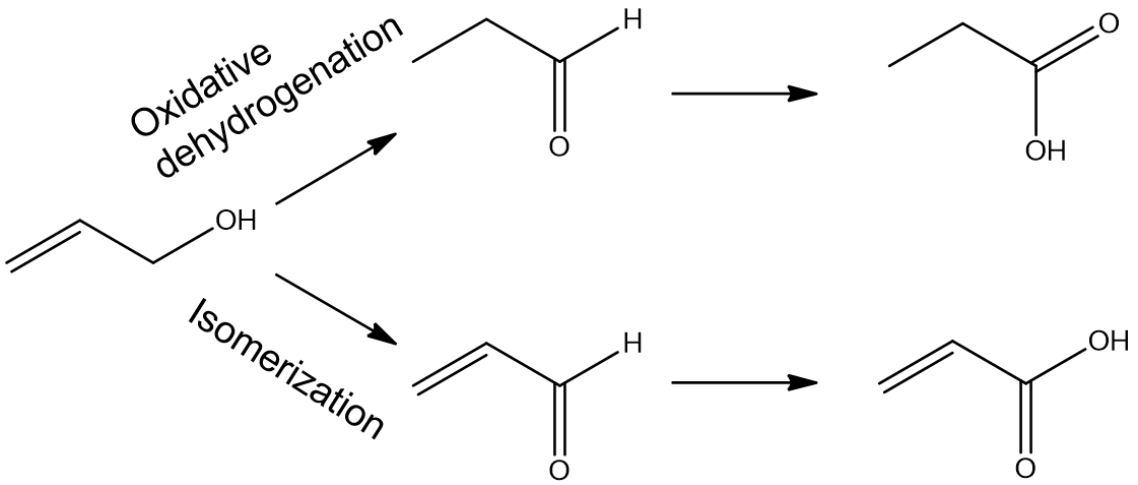

Scheme 1. Reaction pathways for selective oxidation of allyl alcohol to propionic and acrylic acids.

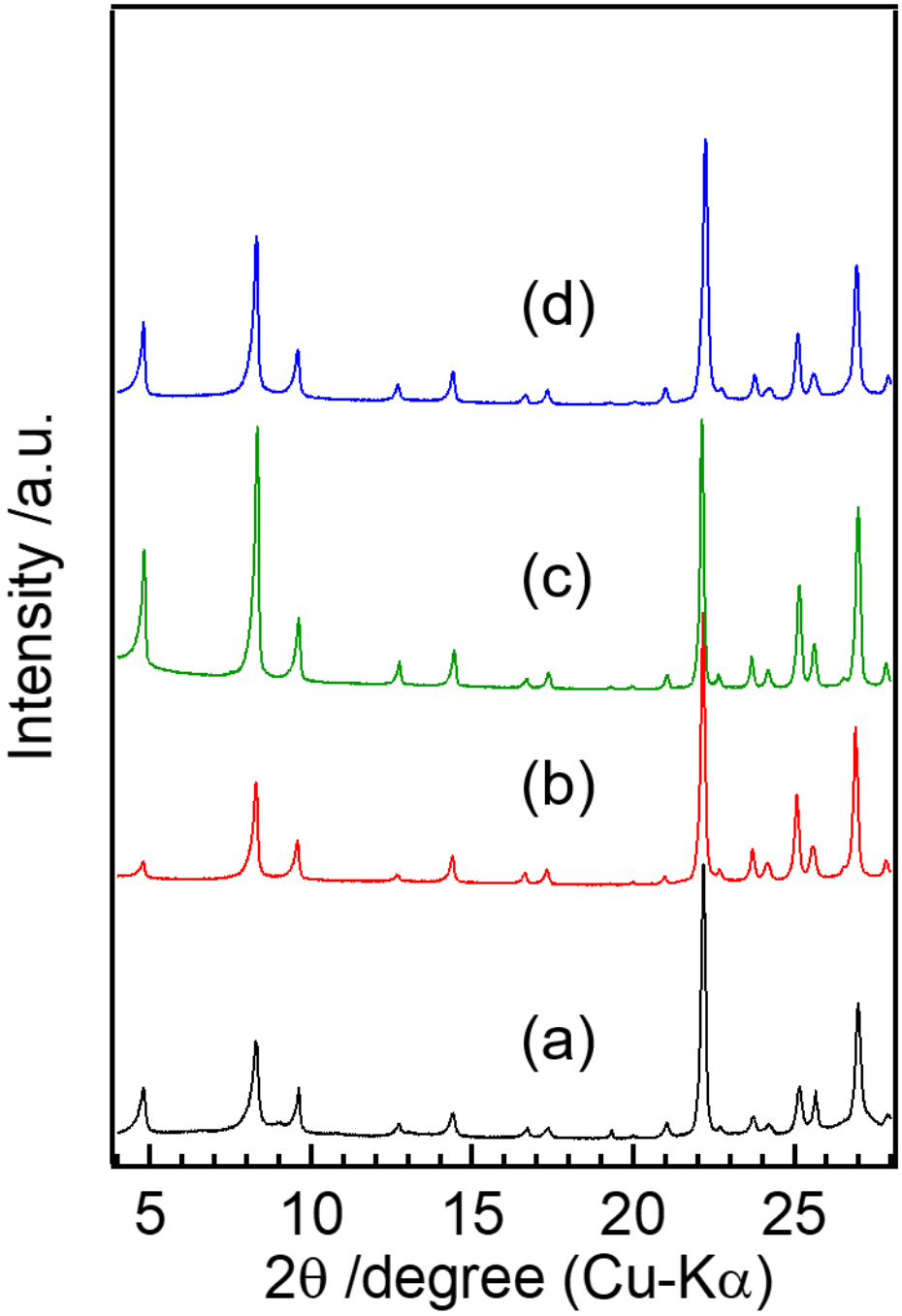

Figure S1. XRD patterns of MoVO (a), MoVFeO (b), MoVCuO (c) and MoVWO (d) after air calcination at 400 °C for 2 h.

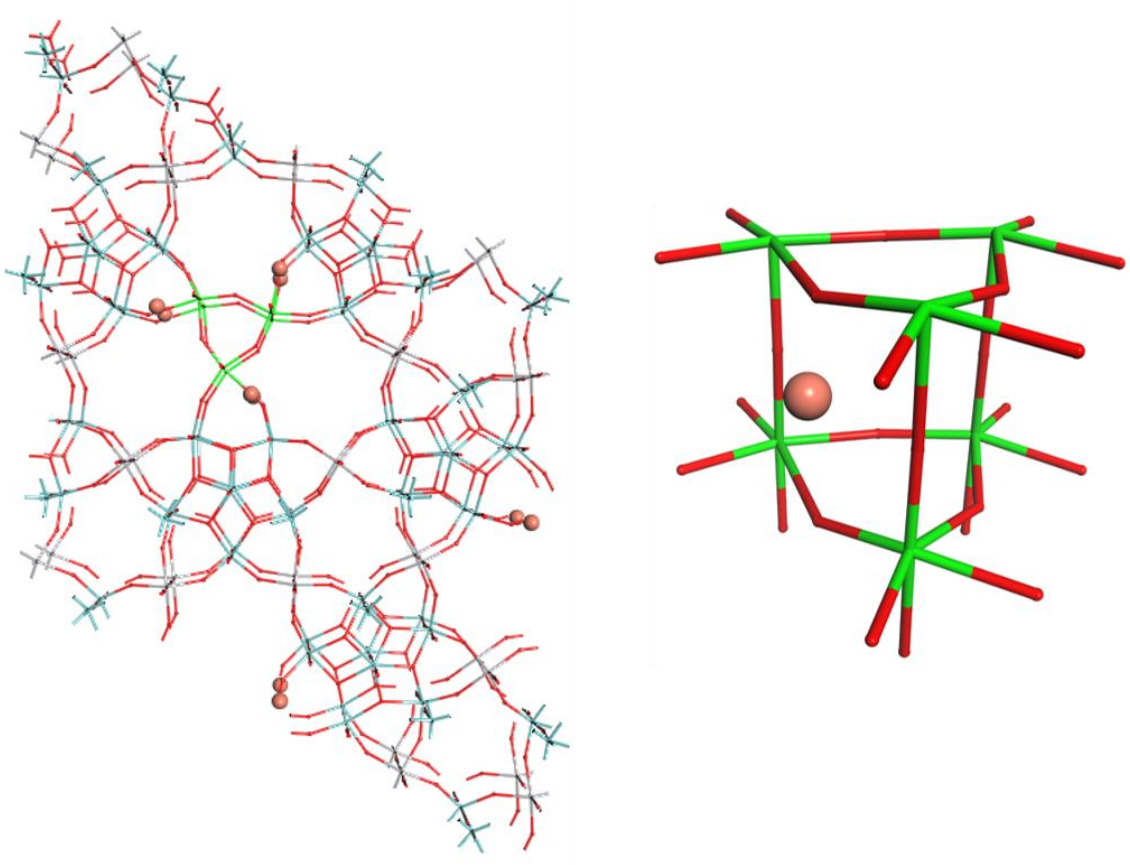

Figure S2. Structural model of MoVCuO obtained after geometry optimization (left figure). Mo, light blue; V, grey; O, red; mixture of Mo and V, dark red; Cu, light green. Local structure around Cu is shown in the right figure.

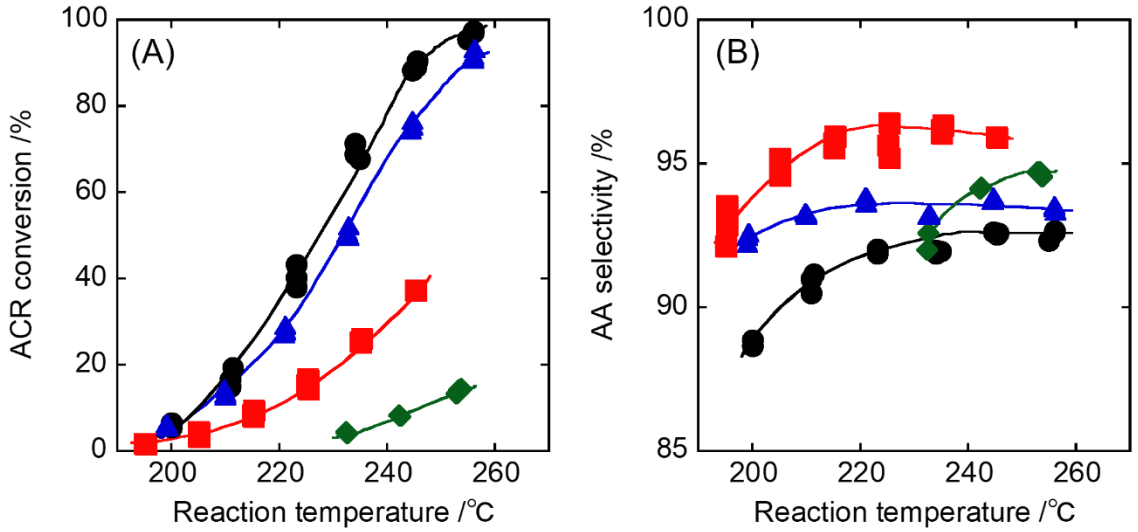

Figure S3. Acrolein conversion (A) and acrylic acid selectivity (B) over MoVO (black circles), MoVFeO (red squares), MoVCuO (green diamonds) and MoVWO (blue triangles) as a function of reaction temperature.

Table S1. Refined parameters and agreement factors of Rietveld refinement of MoVCuO after air calcination at 400 °C for 2 h

	MoVCuO
Crystal system	Trigonal
Space group	P3
a /Å	21.2552
c /Å	4.0179
$\alpha = \beta$ /deg	90
γ /deg	120
V /Å^3	1572.0
Agreement factors	
R_{wp} /%	11.19
R_{wp} (without background) /%	29.39
R_p /%	8.13
Pattern parameter	Pseudo Voigt
Peak shape function	
FWHM	U = 0.44955, V = -0.26009, W = 0.05771
Profile parameter	N_A = 1.05258, N_B = -0.01315
Line shift	
Instrument geometry	Bragg-Brentano
Zero point	-0.79481
Shift#1	0.73210
Shift#2	0.19094
Correction method	Berar-Baldinozzi
Parameter	P_1 = -1.20394, P_2 = -0.30552, P_3 = 2.28298, P_4 = 0.58314

Table S2. Atomic coordinates and occupancy of the framework of MoVCuO after air calcination at 400 °C for 2 h

Site	*x*	*y*	*z*	Occupancy
Mo1	0.16856	0.1325	-0.0763	Mo(1.00)
Mo2	0.22362	0.33956	0.03256	Mo(1.00)
Mo3	0.32529	0.56016	0.11684	Mo(1.00)
Mo4	0.43143	0.44923	-0.02696	Mo(1.00)
Mo5	0.49927	0.28881	-0.0252	Mo(1.00)
V6	0.62687	0.49611	0.06526	Mo(1.00)
Mo7	0.78117	0.6708	-0.03968	Mo(0.10), V(0.90)
V8	0.80513	0.84654	0.15408	Mo(0.14), V(0.86)
Mo9	0.33665	0.26268	0.16038	Mo(1.00)
Cu	0.46847	0.89239	-0.36429	0.28
O1	0.17136	0.1351	0.55072	1.0
O2	0.22833	0.34298	0.56904	1.0
O3	0.31601	0.55555	0.58157	1.0
O4	0.43481	0.44447	0.55627	1.0
O5	0.49188	0.29959	0.55144	1.0
O6	0.62899	0.49199	0.5673	1.0
O7	0.78433	0.6673	0.55397	1.0
O8	0.79976	0.84112	0.56224	1.0
O9	0.33079	0.26912	0.57523	1.0
O10	0.08587	0.13651	0.06415	1.0
O11	0.14399	0.04357	0.07407	1.0
O12	0.12514	0.28273	0.07178	1.0
O13	0.22819	0.24488	0.06128	1.0
O14	0.25218	0.44998	0.07609	1.0
O15	0.27021	0.15963	0.07528	1.0
O16	0.25218	0.59761	0.08137	1.0
O17	0.33037	0.36481	0.07574	1.0
O18	0.3933	0.22299	0.07274	1.0
O19	0.4195	0.52484	0.0907	1.0
O20	0.43307	0.3487	0.06897	1.0
O21	0.52347	0.23466	0.07379	1.0
O22	0.54122	0.49505	0.07658	1.0
O23	0.57857	0.39068	0.07705	1.0
O24	0.69189	0.59013	0.07197	1.0
O25	0.76657	0.74298	0.07075	1.0

Graphical abstract